Tunable Nanostructure and Photoluminescence of Columnar ZnO Films Grown by Plasma Deposition

ARTICLE *in* THE JOURNAL OF PHYSICAL CHEMISTRY C · NOVEMBER 2010

Impact Factor: 4.77 · DOI: 10.1021/jp103902u

6 AUTHORS, INCLUDING:

Johann Toudert
ICFO Institute of Photonic Sciences
54 PUBLICATIONS **351** CITATIONS
SEE PROFILE

Juan Ramon Sánchez-Valencia
Institute of Materials Science of Seville (IC…
31 PUBLICATIONS **370** CITATIONS
SEE PROFILE

Ana Borras
Spanish National Research Council
64 PUBLICATIONS **710** CITATIONS
SEE PROFILE

Agustin R. Gonzalez-Elipe
Spanish National Research Council
432 PUBLICATIONS **7,201** CITATIONS
SEE PROFILE

Tunable Nanostructure and Photoluminescence of Columnar ZnO Films Grown by Plasma Deposition

Pablo Romero-Gómez, Johann Toudert,* Juan R. Sánchez-Valencia, Ana Borrás, Angel Barranco, and Agustín R. Gonzalez-Elipe

Instituto de Ciencia de Materiales de Sevilla (CSIC-Universidad de Sevilla) c/Americo Vespucio 49, 41092 Sevilla, Spain

Received: April 29, 2010; Revised Manuscript Received: October 29, 2010

Nanoporous ZnO thin films presenting a tunable nanostructure and photoluminescence (PL) were grown by plasma enhanced vapor deposition on surface oxidized Si substrates. These films consist of *c*-axis oriented wurtzite ZnO nanocolumns whose topology, crystallinity, and PL can be tuned through the substrate temperature (varied in the 300−573 K range) and the nature of the plasma assistance (pure O_2, O_2/Ar, O_2/H_2, or O_2/N_2 mixture). In particular, these processing parameters influence the intensity of the UV and visible PL bands of the films, related to excitonic and defective radiative transitions, respectively. Increasing the substrate temperature enhances the UV PL and rubs out the visible PL due to the increase of grain size and the removal of interstitial defects. Additional tuning of the intensity ratio between the UV and visible bands can be done by controlling the film thickness. A decrease of the UV PL is observed when the films go thicker, an effect that is likely to be linked to the microstructure of the films rather than to their crystallinity that is improved upon increasing of the film thickness, as seen from PL spectroscopy and XRD measurements. Indeed, a gradient of stress, decreasing from the substrate to the surface, is evidenced and related to a concentration gradient of interstitial defects. The drawbacks of the thickness effect, which prohibits growing thick films with a high optical quality, can be bypassed by growing the films in a O_2/H_2 plasma.

1. Introduction

Due to its wide band gap (∼3.37 eV at room temperature) and high exciton energy (60 meV), ZnO presents an ultraviolet luminescence band[1] that is of prime interest for the realization of electroluminescent diods[2] or room temperature UV lasers.[3] In addition to the UV band related to excitonic radiative recombinations, other luminescence bands have been observed in the visible,[1,4] and their existence has been ascribed to defect-related energy levels between the conduction and valence bands.[4] Depending on the fabrication conditions,[5] native defects (such as oxygen or Zn vacancies[6] and interstitials[7] and oxygen antisites[8]) or extrinsic defects (such as nitrogen[9] or metal[10,11] heteroatoms) can be introduced into the network and thus lead to the control of the electronic structure of the material and consequently to the tailoring of its luminescence response in the visible range. Defects can be located in the volume or at the surface of the material in a proportion that is likely to be controlled by the synthesis process. Surface defects, which are sensitive to the chemical environment of the material,[12] make ZnO a potential candidate for the realization of chemical[13] or gas[14] sensors converting chemical information into electrical[15] or optical signals.[16] Indeed, the existence of a correlation between the intensity of the visible and UV photoluminescence bands has been evidenced,[17] thus suggesting the existence of a certain interaction between excitons and surface defects.[18] A particularly high chemical sensitivity is thus expected in the case of nanostructured materials, in which the surface-to-volume defect ratio may be high. Therefore, much attention has been paid in the last decades to the fabrication and structural characterization of ZnO nanostructures such as nanoparticles,[19] nanoribbons,[20] nanowires,[21] and nanorods.[22] Nanorods can be grown perpendicularly to various substrates in the form of densely packed assemblies of nanostructures presenting a high aspect ratio that provides a high surface to volume ratio.

Among the chemical or physical fabrication routes used to grow ZnO, such as electrodeposition,[23] pulsed laser deposition,[24] hydrothermal,[25] MOVPE,[26] or VLS growth,[27] chemical vapor deposition has allowed the catalyst-free growth of ZnO nanocolumnar films[28,29] and nanorods[30] presenting luminescence bands either in the ultraviolet or visible ranges. Alternatively, it has been shown that, by choosing appropriate precursors and plasma conditions, the use of plasma assistance during the growth of oxide materials by plasma-enhanced chemical vapor deposition (PECVD) is an efficient way to control their composition and nanostructure.[31] However, although some works have been devoted to the PECVD growth of nanocolumnar TiO_2[31,32] thin films, less has been done in this domain concerning ZnO.[30,33,34] Liu et al.[30] investigated the PECVD growth of ZnO nanorods on various crystalline substrates and presented a two-step method for growing ZnO nanorods perpendicular to sapphire substrates with a good optical quality. The growth was performed at 975 K in an O_2 plasma, and the role of the bias voltage, oxygen pressure, and duration of the first deposition step on the growth was underlined. Nevertheless, the influence of other important parameters such as the growth temperature or composition of the plasma has not been studied. In the case of ZnO films, the thickness of deposited material has also previously been shown to play an important role in controlling its structure and optical absorption,[35,36] but its influence on the photoluminescence of CVD-grown ZnO films has not been investigated so far.

This paper reports a study of the influence of growth parameters during the PECVD deposition of nanocolumnar ZnO

* To whom correspondence should be addressed. E-mail: johann.toudert@gmail.com.

10.1021/jp103902u
Published on Web 11/22/2010

thin films on their nanostructure and optical response. By combining a microstructural and nanostructural characterization by scanning electron microscopy (SEM) and X-ray diffraction (XRD) with optical reflectance and photoluminescence (PL) measurements, it is shown that oriented nanocolumnar ZnO films can be grown onto surface oxidized Si at temperature as low as 475 K and that the nature of the plasma, the substrate temperature, and the film thickness strongly influence the topology, crystallinity, and defective state of the material.

2. Experimental Details

ZnO thin films were grown onto surface oxidized Si (100) substrates by PECVD in a plasma reactor with a remote configuration[37] using diethyl zinc ($ZnEt_2$) as zinc precursor. The dosed precursor was brought into the chamber by a dosing line equipped with a mass flow controller and sent onto the substrates through a shower-type dispenser located 3 cm above the sample holder. The dosing line and dispenser were heated at 375 K, and the mass flow controller at 315 K to prevent any condensation in the line walls. A thermocouple was used to monitor the temperature of the sample holder, which can be heated during the deposition using a halogen lamp. The microwave plasma source (SLAN, Plasma Consult GMbh) is coupled to the reaction chamber and separated from it by a grounded grid located 10 cm above the sample holder. This grid avoids the microwave heating of the substrates and minimizes ion bombardment effects.[38] Total pressure during deposition was 4×10^{-3} Torr. The plasma source was operated at a power of 400 W with either pure O_2 or O_2/H_2 (in a ratio 80%/20%), O_2/Ar (10%/90%), or O_2/N_2 (10%/90%) mixtures as plasma gas. In all cases, the samples were treated with pure O_2 plasma in standard conditions of pressure, both before and after film deposition, in order to clean the substrates and the deposited films.[39] The synthesis of the films was carried out at a substrate temperature tuned between room temperature and 575 K. The thickness of the films was estimated ex situ by fitting the optical reflectance spectra as measured in the 500−900 nm range at normal incidence with a Bruker spectrometer equipped with a confocal objective. Around 40 samples were prepared to ascertain the influence of the nature of the plasma, substrate temperature, and sample thickness on the nanostructure and optical response of the films. Since many of these samples present only a slightly different optical response, we focused the nanostructural and microstructural study on selected samples, whose preparation conditions and thickness are presented in Table 1. The samples were labeled in order to present clearly the value of the three growth parameters that have been varied in this study. For instance, the sample grown with a mixture of O_2 and Ar, at a substrate temperature of 475 K and presenting a thickness of 700 nm, will be denoted as "O_2/Ar 475 K 700 nm".

The surface and in-depth microstructure of the films have been observed by plan-view and cross-sectional SEM respectively, using a Hitachi S5200 field emission microscope operated at 5.0 keV. The crystal structure of the films has been studied by XRD in a Siemens D5000 spectrometer operated in the $\theta-2\theta$ configuration and using the Cu Kα radiation as an excitation source. Continuous wave photoluminescence (PL) measurements were carried out at room temperature in the front face configuration using a Horiba Jobin Yvon Fluorolog3 fluorimeter equipped with a 450 W Xe lamp and two monochromators. The excitation monochromator, located between the source and the sample, was used to select the wavelength of the pumping beam, which was set at 280 nm. The light emitted by the sample was collected by a PMT detector through the emission monochromator. PL measurements were performed by scanning the emission wavelength between 350 and 800 nm with a 5 nm monochromator step. The system was equipped with filters in order to remove stray light effects, and the measured spectra were corrected from variations of the pumping intensity. All the samples were measured in identical experimental conditions in order to compare their PL intensities. Reflectance spectroscopy of the films of the "thickness" series was measured at room temperature with a Woollam VASE ellipsometer at a 25° incidence angle, with a S-polarized incident beam (i.e., close to the front face PL measurement conditions) in the 250−1000 nm range with a 2 nm monochromator step.

TABLE 1: Label, Plasma Conditions, and Substrate Temperature during the Growth of the ZnO Films and Thickness as Determined by Optical Reflectance Measurements[a]

sample label	plasma condition (%O_2, %H_2, %Ar, %N_2)	temperature T (K)	thickness (nm)
O_2 300 K 550 nm	(100, 0, 0, 0)	300	550
O_2 410 K 450 nm	(100, 0, 0, 0)	410	450
O_2 475 K 400 nm	(100, 0, 0, 0)	475	400
O_2 575 K 500 nm	(100, 0, 0, 0)	575	500
O_2 410 K 200 nm	(100, 0, 0, 0)	410	200
O_2 410 K 870 nm	(100, 0, 0, 0)	410	870
O_2 410 K 1270 nm	(100, 0, 0, 0)	410	1270
O_2 410 K 1750 nm	(100, 0, 0, 0)	410	1750
O_2/H_2 475 K 800 nm	(80, 20, 0, 0)	475	800
O_2/Ar 475 K 700 nm	(10, 0, 90, 0)	475	700
O_2/N_2 475 K 300 nm	(10, 0, 0, 90)	475	300

[a] Due to the crudeness of the model used to fit the reflectance data, errors of a few tens of nanometers are expected in the determination of the thickness.

3. Topology, Crystal Structure and Optical Response of the ZnO Films

3.1. Influence of the Growth Temperature. Figure 1 displays SEM cross-sectional views and plan views (insets) showing respectively the in-depth and surface topology of the films grown with a O_2 plasma at various substrate temperatures. It can be seen from the cross-sectional views that the films present a columnar microstructure whatever the substrate temperature. More precisely, they consist of nanocolumns oriented almost perpendicularly to the substrate, presenting rough lateral faces and whose apparent width increases from the interface with the substrate to the film surface. At a given distance from the substrate, the apparent width of the nanocolumns is shown to increase with the growth temperature. The growth temperature also influences the in-plane morphology of the material. Indeed, the in plane projected shape turns from elliptic without preferential orientation to almost circular when increasing the substrate temperature from 300 to 475 K. The film grown at 575 K (micrograph not shown) presents a topology very similar to the one grown at 475 K.

Figure 2a shows the XRD patterns of the same film series, together with that of a ZnO wurtzite powder displaying three peaks located at 31.8°, 34.45°, and 36.15° corresponding to the (100), (002), and (101) planes, respectively, of stress-free ZnO.

The presence of the three peaks in the XRD patterns of the film grown at 300 K proves that this film consists of wurtzite ZnO. In contrast with the ZnO wurtzite powder, the most intense peak for this film is the one related to the (002) planes, testifying for a preferential crystal orientation with the *c*-axis of the hexagonal wurtzite elementary cell perpendicular to the sub-

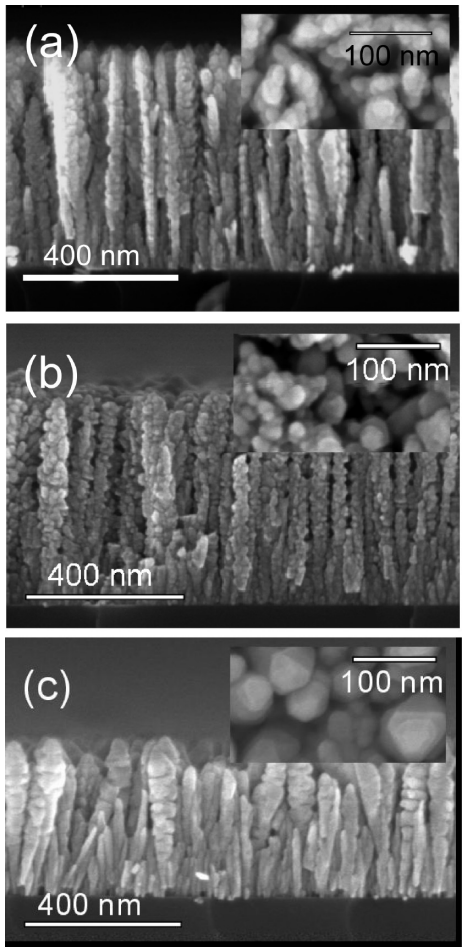

Figure 1. SEM cross-sectional and plan-view (insets) micrographs of the ZnO films grown with a O_2 plasma and at different substrate temperatures: (a) 300 K (O_2 300 K 550 nm); (b) 410 K (O_2 410 K 450 nm); and (c) 475 K (O_2 475 K 400 nm).

strate. The XRD patterns of the films grown at higher temperatures only display the (002) peak, showing that the preferential crystal orientation is improved upon increasing of the growth temperature. A narrowing of the (002) peak is also observed as a result of a better crystallinity along the direction perpendicular to the substrate. Indeed, as shown in Figure 2b, the crystal domain size extracted from the full-width at half-maximum of the (002) peak using the Scherrer equation increases from 42 to 100 nm when the temperature increases from 300 to 575 K. It can also be seen from the XRD patterns that the (002) peak shifts toward higher angle values when the temperature increases. This evolution is presented in Figure 2c, where it can be seen that the (002) peak of the films grown at room temperature and 410 K (475 and 575 K) appears at a lower (respectively higher) angle when compared to the stress-free ZnO powder. Similar changes have been observed upon annealing of ZnO films by Fang et al.[40] and attributed to a transition from a state of tensile stress to a state of compressive stress along the *c*-axis.

From the previous SEM and XRD results, it is apparent that ZnO nanocolumns with a preferential *c*-axis crystal orientation are formed at relatively low temperatures such as 300 K on silicon substrates presenting an amorphous oxidized surface. Such a *c*-axis oriented growth on surface oxidized silicon and other amorphous surfaces has been observed previously and discussed in terms of the minimization of the free energy of the growing crystals.[41] The existence of separated nanocolumns could result from the formation of *c*-axis oriented ZnO nuclei (following a Volmer−Weber-like growth mechanism) in the early growth stages of the film.[30] These nuclei may act as seeds for the preferential growth of the columns that, additionally, may be influenced by shadowing and electric field effects.[30] The larger width and rounder in-plane projected shape of the nanocolumns as seen by SEM when the growth temperature is increased would thus reflect a faster diffusion of matter on the substrate during the early stages of growth. Indeed, the higher the temperature, the bigger and rounder will be ZnO nuclei. Increasing the substrate temperature has also been shown to improve the crystalline quality of the film through the increase of the grain size and to affect its stress state, which turns from tensile to compressive. Among the causes of stress of thin films, lattice mismatch[42] with the substrate and presence of interstitial defects are known to induce tensile stress. In our case, since the substrates are surface oxidized silicon, no epitaxial growth is expected, and the tensile stress in the films that were grown at room temperature and 410 K should be due to the presence of interstitial defects. At a higher temperature, due to enhanced mobility of the atoms during the growth, these defects could be removed, thus minimizing tensile stress. The appearance of

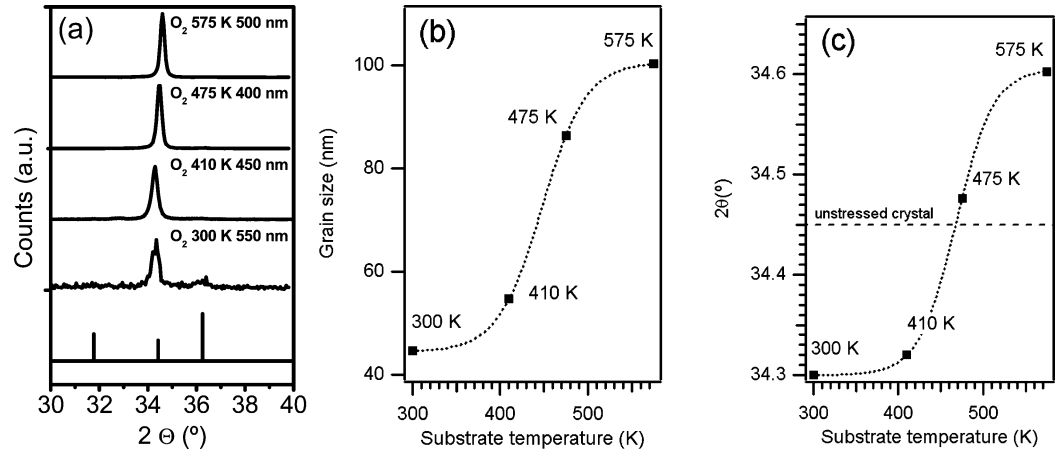

Figure 2. (a) $\theta-2\theta$ X-ray diffraction spectra of the films grown with a O_2 plasma at various substrate temperatures, (b) evolution of the ZnO crystal size along the vertical axis determined from the (002) peak width, and (c) evolution of the angular position of the (002) wurtzite diffraction peak as a function of the substrate temperature. The dotted lines in (b) and (c) are a guide for the eye. The dashed line in (c) represents the angular position of the (002) peak of a stress-free ZnO wurtzite crystal, taken from JCPDS tables.

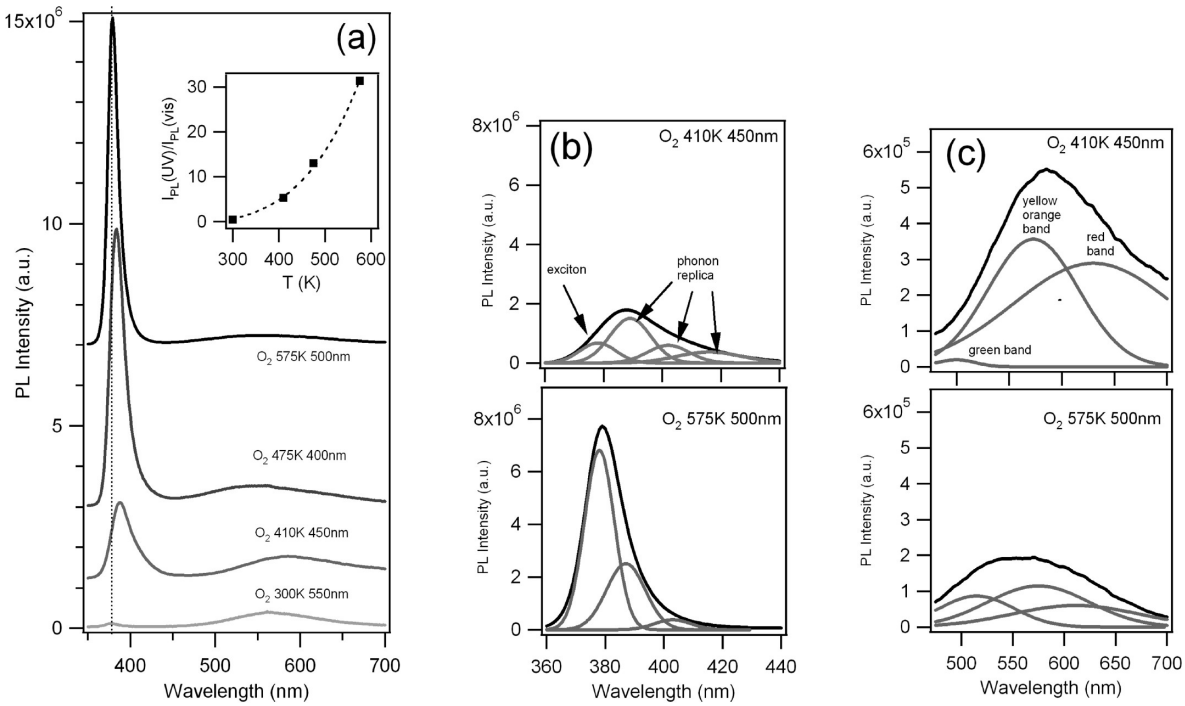

Figure 3. (a) Room temperature photoluminescence spectra of the thin films grown with a O_2 plasma at different substrate temperatures (The vertical dotted line representing the 378 nm wavelength has been drawn in each figure as a guide to the eye) and (b) spectra of the UV photoluminescence of two selected films and their corresponding Gaussian components. The peak at 378 nm is attributed to the recombination of free excitons and the others to phonon replicas. (c) Visible photoluminescence spectra of two selected films and their corresponding Gaussian components.

compressive stress in thin films that have a thermal expansion coefficient higher than that of the substrate (as occurs for the ZnO/Si system) is linked with the rapid cooling of the film/substrate system after the synthesis.[40]

The room temperature PL spectra of the films grown with a O_2 plasma at various substrate temperatures are gathered in Figure 3a. It can be seen in this figure that the films present two photoluminescence bands, a narrow one in the UV range (peaking around 380 nm) and a broad one in the visible range (in the 500−700 nm range). The former is generally attributed to radiative excitonic recombinations[1,43] and the latter to radiative transitions involving defect-related energy levels located in the bandgap[1,4,44] (transition between two defect levels, between a defect level and the valence band, or between the valence band and a defect level). The PL spectrum is already dominated by the UV band at a growth temperature of 410 K, suggesting that films of excellent optical quality can be obtained in our PECVD system at relatively low temperatures. The intensity of the UV (visible) PL band increases (decreases) when the films are grown at higher temperature, thus inducing an increase of the "optical quality factor" (inset in Figure 3a) defined in this paper as the ratio between the maximum of the UV peak and the intensity at 575 nm. Such an increase of the optical quality factor can be correlated to the improvement of the crystal quality as evidenced by SEM and XRD. Indeed, the elimination of defects is known to produce a decrease of the intensity of the visible PL band. At the same time, the increase of the grain size[45,46] and thus the decrease of the surface to volume ratio should contribute to the enhancement of the UV PL peak by decreasing the probability of nonradiative de-excitation processes at the surface of the grains.

In addition to the intensity, it can be seen in Figure 3a that the spectral position and shape of the UV and visible PL bands depend on the growth temperature. This dependence has been studied by performing a more accurate analysis of the PL spectra of two selected films: "O_2 410 K 450 nm", and "O_2 575 K 500 nm". The UV PL band is usually attributed to radiative excitonic recombinations.[42] When photoluminescence is measured at low temperature, peaks related to the recombination of free excitons followed by phonon replicas, bound excitons, and even surface excitons can be resolved.[41] At room temperature, only subsist the contributions of the free exciton and phonon replicas that merge due to thermal damping. The UV PL band measured at room temperature is thus usually considered as the convolution of one peak related to the direct radiative recombination of the exciton and additional peaks linked to phonon replicas located at longer wavelengths. The relative weight of the exciton peak is usually affected by the crystal quality of the material. The PL band of a perfect crystal is governed by the exciton peak, whereas those of a defective and polycrystalline material will present stronger contributions from the phonon replicas.[47] In addition, in the case of confined structures such as nanorods, different waveguiding behaviors of the exciton and phonon replica luminescence may affect the emission pattern of the material.[48] In order to evaluate the weight of the different excitonic contributions in the spectra of the two films, their UV PL band was fitted with a sum of Gaussian functions, centered at 378 nm (free-excitonic contribution), 389, 402, and 416 nm (phonon replicas). Figure 3b shows the UV PL bands of the two samples and in each case the corresponding Gaussian components. The phonon replicas dominate in the case of the "O_2 410 K 450 nm" film for which the excitonic contribution is almost absent. The weight of the free-excitonic contribution increases with the growth temperature, inducing an apparent blue-shift of the UV PL band. These results are in agreement with XRD measurements showing that the crystal quality is improved (grain size increases) upon increasing the growth temperature.

The visible PL band is usually attributed to radiative recombination events involving defect levels located in the

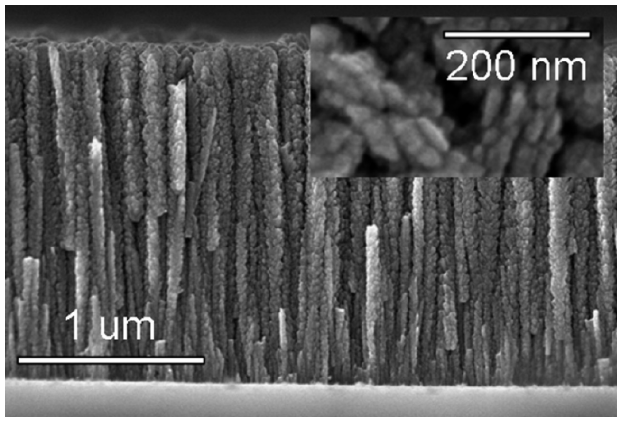

Figure 4. SEM cross-sectional view of the O_2 410 K 1730 nm film (inset: SEM surface view).

bandgap.[1,4,42] Due to the high number of possible defect levels, the visible PL bands generally present a complex spectral shape making the extraction of structural data from the spectra an uneasy task. Nevertheless, in the absence of trapped heteroatoms, it has been observed[49−51] that ZnO films presenting a green luminescence band (peaking between 480 and 520 nm) are Zn-rich and that those presenting a yellow-orange luminescence band (peaking between 550 and 600 nm) are O-rich. Red or near infrared luminescence bands whose origin remains unclear have also been reported. Fits of the visible PL bands of the two films have thus been performed with the sum of 3 Gaussian functions centered at around 520, 580, and 650 nm. The experimental bands, which present significantly different spectral shapes are shown in Figure 3c together with their corresponding 3 Gaussian components. The visible band of the "O_2 410 K 450 nm" is dominated by the yellow band, suggesting that this film is O-rich. The absolute and relative intensities of this band are strongly reduced upon increasing the growth temperature. It can thus be proposed from these results and those of XRD that the "O_2 410 K 450 nm" is under tensile stress due to the presence of interstitial oxygen in the crystal lattice. Additionally, the low intensity of the oxygen-linked band in the visible PL spectra of the "O_2 575 K 500 nm" film may reflect a lower amount of interstitial oxygen in this film.

3.2. Influence of the Film Thickness. Figure 4 shows the cross-sectional SEM micrograph of the thickest film of this study ("O_2 410 K 1750 nm"). Almost 1.5 μm high, well-defined, and vertical columns can be seen, suggesting that the columnar growth is preserved even in the case of thick films. Moreover, the projected width of the columns increases from the substrate to the film surface, thus inducing a decrease of the porosity, whereas the lateral roughness of the columns increases.

Figure 5a presents the XRD patterns of the samples grown at a 410 K temperature with a O_2 plasma presenting different thicknesses ranging from 200 to 1750 nm. All of them are dominated by the (002) peak, whose intensity increases with the thickness, showing that the material keeps growing with the *c*-axis perpendicular to the substrate whatever the deposited thickness. Moreover, it can be seen that the (002) peak shifts toward higher angles when the thickness is increased. It is centered at 34.28° for the 200 nm thick film and at 34.41° for the 1750 nm thick film, suggesting that the average stress state of the film turns from tensile to unstressed when the thickness increases. Looking more precisely at the (002) peaks, it can be seen that they are not symmetric, in contrast with the diffraction peaks of perfect crystals, and that their asymmetry increases with the film thickness. Fits of these peaks performed using a sum of Lorentz functions (see S1 of the Supporting Information) suggest that the ZnO films under study can be considered as a material with a vertically decreasing gradient of stress. As a typical example, the "O_2 410 K 1750 nm" film would present tensile stress close to the substrate and be almost unstressed close to the surface.

Figure 5b presents the reflectance spectra of the films together with their corresponding best fit. Fitting was performed using

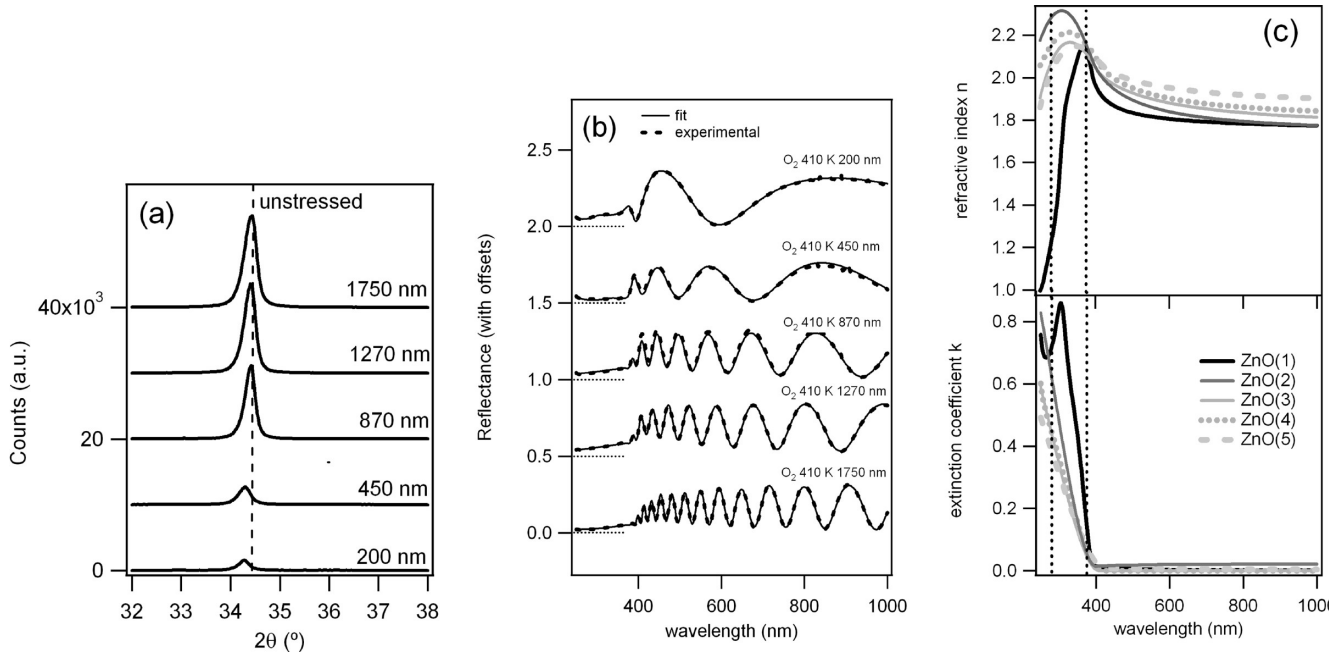

Figure 5. (a) $\theta-2\theta$ X-ray diffraction spectra of films presenting different thicknesses grown with a O_2 plasma at a substrate temperature of 410 K. The vertical dashed line represents the angular position of the (002) peak of stress-free ZnO wurtzite bulk crystal. (b) Reflectance spectra of the five films and corresponding best fits, (c) *n* and *k* spectra extracted for the five effective ZnO layers using the multilayer structures depicted in Table 2. The vertical dotted lines correspond to wavelengths of 280 nm (excitation wavelength during PL experiments) and 375 nm (typical of the UV PL band).

TABLE 2: Structures Used for Fitting Optical Reflectance Spectra of the Films of the "Thickness Series"

sample	structure (thicknesses for the best fit)
O_2 410 K 200 nm	$Si/ZnO(1)_{235\ nm}/roughness_{25\ nm}$
O_2 410 K 450 nm	$Si/ZnO(1)_{209\ nm}/ZnO(2)_{240\ nm}/roughness_{39\ nm}$
O_2 410 K 870 nm	$Si/ZnO(1)_{210\ nm}/ZnO(2)_{204\ nm}/ZnO(3)_{514\ nm}/roughness_{34\ nm}$
O_2 410 K 1270 nm	$Si/ZnO(1)_{247\ nm}/ZnO(2)_{43\ nm}/ZnO(3)_{535\ nm}/ZnO(4)_{289\ nm}/roughness_{33\ nm}$
O_2 410 K 1750 nm	$Si/ZnO(1)_{227\ nm}/ZnO(2)_{195\ nm}/ZnO(3)_{468\ nm}/ZnO(4)_{393\ nm}/ZnO(5)_{483\ nm}/roughness_{42\ nm}$

the WVASE32 (Woollam) software. In order to account for a possible in-depth gradient of refractive index n and extinction coefficient k, each film was described as a stack of effective medium layers, the number of which increasing with the film thickness, as depicted in Table 2. The top layer of each stack was an effective medium averaging the optical properties of void and the underlying material, in order to take the surface roughness into account. The n and k of the underlying layers were described as the sum of a Cauchy law with Urbach absorption tail and a Tauc−Lorentz oscillator. An excellent fit was obtained for the thinnest film ("O_2 410 K 200 nm") considering it as a ZnO(1)/roughness bilayer (Table 2). Fitting of the reflectance spectrum of the "O_2 410 K 450 nm" film was made using a [ZnO(1)/ZnO(2)/roughness] trilayer model, where the ZnO(1) layer had the same optical properties as that of the "O_2 410 K 200 nm" film. For the "O_2 410 K 870 nm", "O_2 410

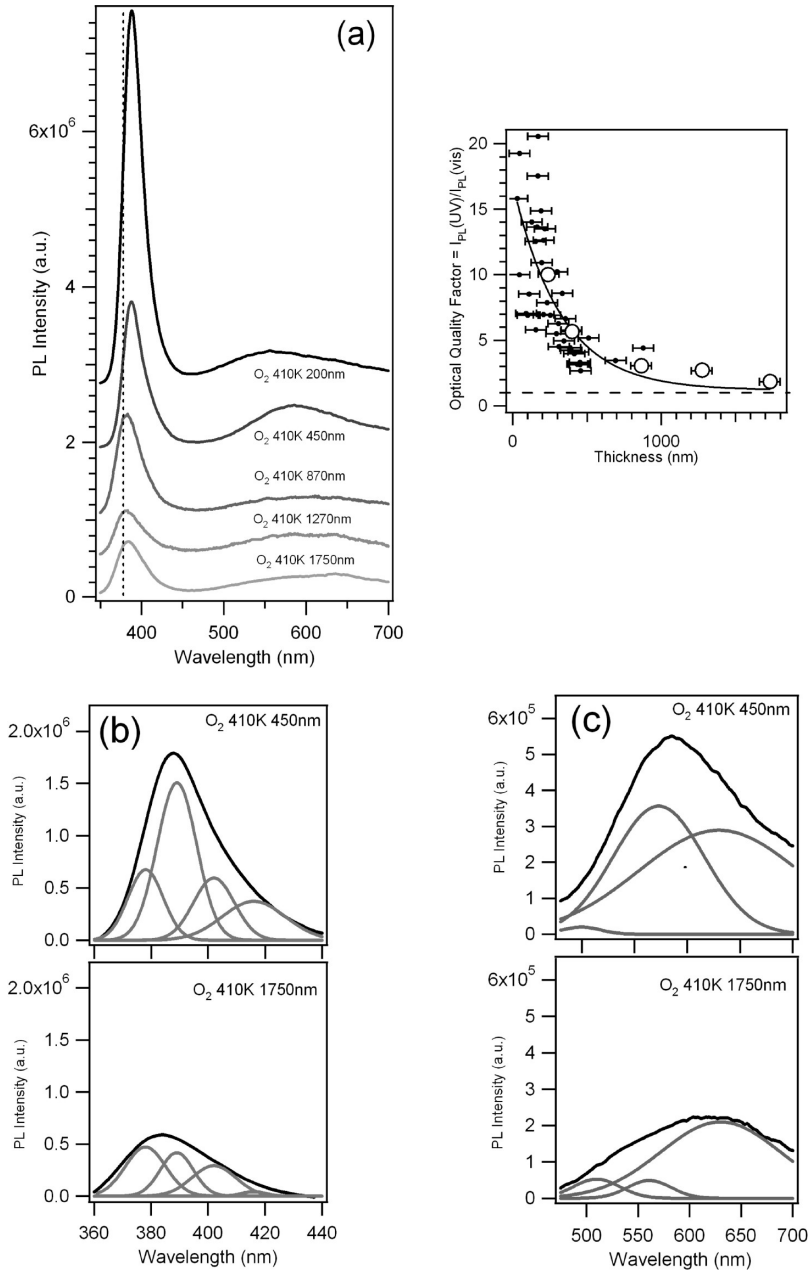

Figure 6. (a) Room temperature photoluminescence spectra of the thin films grown with a O_2 plasma at 410 K presenting different thicknesses and optical quality factor evolution versus thickness, (b) spectra of the UV photoluminescence of two selected films and their corresponding Gaussian components, and (c) visible photoluminescence spectra of two selected films and their corresponding Gaussian components.

K 1270 nm", and "O_2 410 K 1750 nm" films, fitting was performed with four, five, and six layers, respectively, thus permitting to extract iteratively the *n* and *k* of the ZnO(3), ZnO(4), and finally ZnO(5) layers.

Figure 5c shows the *n* and *k* spectra of the five ZnO(*i*) layers constituting the "O_2 410 K 1750 nm" film, revealing an in-depth gradient of optical properties. The refractive index in the visible increases from 1.8 to 2 from the susbtrate to the surface, an effect that can be related to the decrease of porosity as observed from the SEM cross-sectional view. Meanwhile, the slope of the UV absorption of the material decreases, the most significant evolution occurring in a 500 nm thick region starting from the substrate. Similar changes were observed by Malandrino et al.[52] after annealing nanoporous polycrystalline ZnO films and attributed to an improvement of the crystal structure (reduction of the amorphous tissue and the presence of grain boundaries causing lower polarizability per unit volume). XRD and reflectance measurements thus point out an improvement of the crystal quality (less stress, better crystalline order) with the distance to the substrate.

It can be seen in Figure 6a, which shows the full PL spectra of the five films, that the intensity of both PL bands (the UV band and the visible band) decrease as the film thickness increases. The faster decrease of the UV PL intensity provokes a decrease of the optical quality factor (as shown in the inset of the same figure). At this point, it has to be highlighted that, due to the absorption of the pump beam at 280 nm, the probe depth of PL measurements is estimated (from simulations based on the *n and* k spectra shown in Figure 5c) to increase from around 100 nm (for the 200 nm thick film) to 200 nm for the 1750 nm thick film. This argument is very important for interpreting the influence of the film thickness on the PL. Indeed, in the case of thick films (thickness >100 nm), only the outmost surface layers of the films are probed, in contrast with XRD or cross-sectional SEM measurements that probe the whole material. Deconvolution of the visible PL peaks (Figure 6c) shows that the contribution of the yellow-orange band in the visible PL (Figure 6c) decreases when the film thickness increases. From this result, it can be proposed that the surface zone of the "O_2 410 K 1750 nm" film presents a better stoichimetry than the one of the "O_2 410 K 450 nm" film (that presents a PL typical of an excess of oxygen). Correlation with XRD data suggests that the vertical gradient of stress, with lower (higher) stress close to the surface of the film (film/substrate interface), is due to a vertical gradient of interstitial oxygen. Deconvolution of the UV PL peaks (Figure 6b) shows that the relative weight of the excitonic contribution increases with the film thickness. This could be a consequence of a vertical gradient of crystal order following the gradient of stress. Since the UV PL intensity and optical quality factor decrease upon depositing more material (Figure 6a) while the crystal order and stoichoimetry of the surface layer improve, another parameter should influence the UV PL band. At the emission wavelengths of the free exciton and phonon replicas (between 378 and 420 nm), the absorption coefficient of ZnO (Figure 5c) is very low (below 0.02) whatever the depth, thus permitting to discard a possible role of reabsorption of the emitted light in our measurement conditions (excitation and collection at near-normal incidence). A more probable interpretation of the "thickness effect" (on the intensity of the UV PL) may involve scattering of the emitted light by the rough lateral and top faces of the nanocolumns. An increasing gradient of lateral roughness has effectively been observed (from the substrate to the surface) by SEM and thicknesses of 25 and 42 nm were obtained for the roughness layer of the thinnest and thickest film, respectively. The decrease of the UV PL (collected at near normal incidence) when thickness increases could therefore result from scattering of light away from the collection direction.

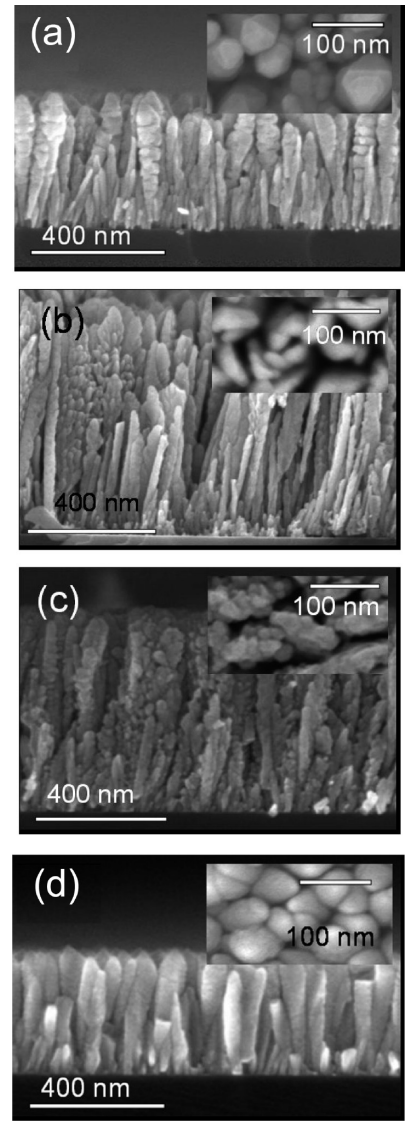

Figure 7. SEM cross-sectional and plan-view (insets) micrographs of the ZnO films grown at 475 K substrate temperature and with different plasmas: (a) O_2 plasma (O_2 475 K 400 nm); (b) O_2/H_2 plasma (O_2/H_2 475 K 800 nm); (c) O_2/Ar plasma (O_2/Ar 475 K 700 nm); and (d) O_2/N_2 plasma (O_2/N_2 475 K 300 nm).

3.3. Influence of the Plasma Composition. Figure 7 presents the SEM cross-sectional and plan-view micrographs of the films grown at a 475 K substrate temperature and different nature of the plasma gas. A columnar nanostructure is observed from the cross-sectional views whatever the plasma conditions, which however influence significantly the topology of the nanocolumns. In particular, at a given distance from the substrate, a smaller width is observed for the nanocolumns grown with O_2/H_2 and O_2/Ar plasmas. Let us remark that the columns grown in O_2/H_2 are particularly smooth. The plan-view micrographs also demonstrate the role of the plasma on the in-plane structure of the films. An almost circular in-plane projected shape is reported in the case of nanocolumns grown with O_2 and O_2/N_2 plasmas, whereas those grown with O_2/H_2 and O_2/Ar plasmas present an elliptic projected shape without specific orientation.

Figure 8a shows XRD patterns of the films grown at 475 K with plasmas of different nature. As in the case of the films

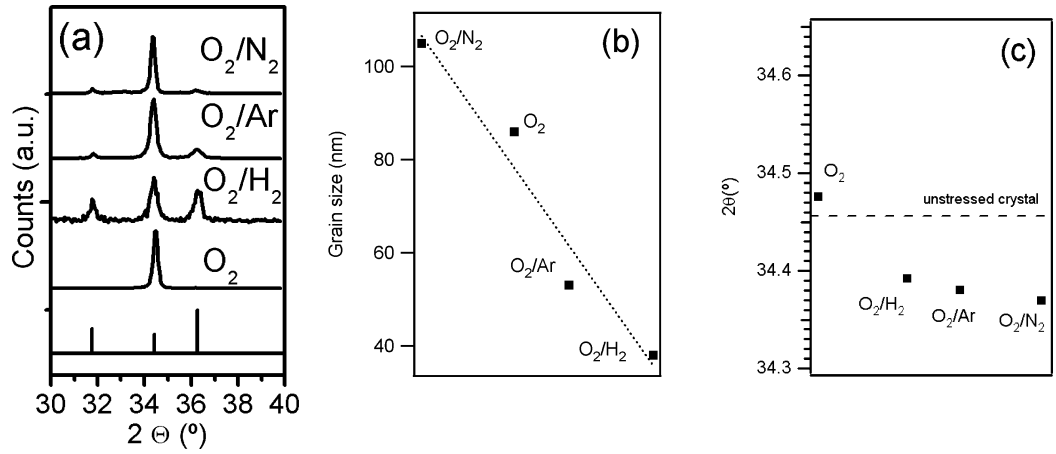

Figure 8. (a) $\theta-2\theta$ X-ray diffraction spectra of the films grown at a 475 K substrate temperature and with different compositions of the plasma. (b) Evolution of the ZnO crystal size along the vertical axis determined from the (002) peak width as a function of the plasma composition. The dotted line is a guide for the eye. (c) Evolution of the angular position of the (002) wurtzite diffraction peak as a function of the plasma composition. The dashed line represents the angular position of the (002) peak of stress-free wurtzite ZnO crystal.

grown with a O_2 plasma, the films consist of ZnO in an hexagonal wurtzite phase with a preferential orientation of the *c*-axis perpendicularly to the substrate. The crystalline organization can be monitored through the degree of preferential orientation of the *c*-axis perpendicularly to the substrate (reflected by the relative intensity of the diffraction peaks) and by the size of the crystal domains along the [002] direction (shown in Figure 8b), which are both affected by the nature of the plasma. Films grown with O_2 and O_2/N_2 plasmas display a bigger size of crystal domains and a more pronounced preferential orientation and thus a better crystalline organization than those grown with O_2/Ar or O_2/H_2 plasmas. Moreover, as seen in Figure 8c, the (002) peaks of the films grown with O_2/Ar, O_2/N_2, and O_2/H_2 plasmas are slightly shifted toward lower angles when compared to the unstressed value. This suggests that, in contrast with the film grown in O_2, tensile stress (that could be ascribed to the presence of interstitial defects) still exists.

The different micro- and nanostructure of the films prepared with the aforementioned plasma gas compositions are likely the result of a different growing mechanism occurring in each case. In fact, the growing processes must be very dependent on the nature of the intermediate species of Zn formed in each case and/or on the generation of lattice defects by the interaction of the growing film with activated species of the plasma gas (e.g., Ar*, H*, N*, N_2*, etc.). Note for example the presence of relatively heavy Ar ions bombarding the growing films in the case of mixtures O_2/Ar mixtures. Such dependence has been reported previously for TiO_2 grown by PECVD where the different decomposition degree of the precursor with plasmas of O_2 or mixtures O_2/Ar and O_2/N_2 leads to the formation of films with quite different nanostructures and microstructures.[31]

It can be seen in Figure 9a that the film grown in a O_2/N_2 plasma presents no UV PL peak but a broad band in the 400−500 nm range that might be linked to the presence of donor levels below the valence band induced by the incorporation of nitrogen to the film. Growing the films in a O_2/H_2 plasma enhances the intensity of the UV PL when compared to a film grown in O_2. A very high optical quality factor is obtained (see inset of Figure 9a) for this film, despite its 800 nm thickness and small grain size. Indeed, in addition to previous XRD data, the UV PL of this film (Figure 9b) presents a strong phonon replica, and its visible PL is markedly influenced by the yellow-orange band characteristic of O-rich materials (see note in S2 of the Supporting Information). The intense UV PL of this film might arise from the passivation of active recombination centers by H_2 during the growth,[53] which is a feature that would contribute to suppress nonradiative de-excitation routes of the exciton and to enhance the UV luminescence. One can note the smoothness of the columns grown in a O_2/H_2 plasma, which may prevent scattering of the emitted light (in contrast with the columns grown with a O_2 plasma), thus leading to a better collection of the UV PL in our measurement conditions.

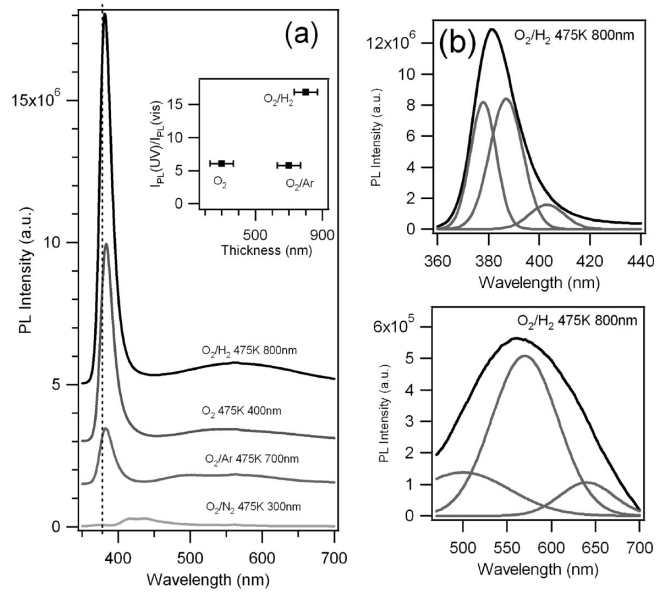

Figure 9. (a) Room temperature photoluminescence spectra of the thin films grown with at 475 K with various plasmas and (b) spectra of the UV photoluminescence and visible photoluminescence spectra of a film grown in a O_2/H_2 plasma and the corresponding Gaussian components.

4. Conclusions

By means of the PECVD technique at substrate temperature as low as 475 K, it has been possible to grow nanocolumnar ZnO thin films with a preferential *c*-axis orientation, low concentration of defects, and strong UV PL. Films microstructure, crystallinity, and PL can be tuned both in the UV and visible ranges by modifying the substrate temperature, nature of the plasma gas, and film thickness. Enhancement of the UV PL is obtained upon increasing the substrate temperature and

attributed to the improvement of the crystal order. In a O_2 plasma, growing thicker films induces a decrease of the UV PL, showing that it is necessary to limit the thickness of deposited material to obtain films of optimal optical quality. This "thickness effect" is likely to be linked to the microstructure of the films rather than to their crystalline structure. The thickness limitation can be overcome by growing the material in a O_2/H_2 plasma, in which thick films with a high optical quality factor were obtained. In addition, the correlation between the data extracted from XRD, reflectance, and PL spectra permits getting a deep insight into the in-depth structure of the films, showing that these two techniques can be combined for a precise nondestructive characterization of ZnO films.

Acknowledgment. This work was supported by the MICINN (projects FUNCOAT CDS2008-0023, MAT20010-21218) and Junta de Andalucía (Project P09-TEP-5283). J.T. acknowledges the Spanish Ministry for Research and Innovation for financial support (Juan de la Cierva Grant JCI-2009-05098).

Supporting Information Available: Lorentz deconvolution of the (002) diffraction peaks of the films (S1), and composition of the plasma (S2). This material is available free of charge via the Internet at http://pubs.acs.org.

References and Notes

(1) Djurisic, A. B.; Leung, Y. H. *Small* **2006**, *2*, 944.
(2) Konenkamp, R.; Word, R. C.; Godinez, M. *Nano Lett.* **2005**, *5*, 2006.
(3) Hung, M.; Mao, S.; Feick, H.; Han, H.; Wu, Y.; Kind, H.; Weber, E.; Russo, R.; Yang, P. *Science* **2001**, *292*, 1897.
(4) Djurisic, A. B.; Leung, Y. H.; Tam, K. H.; Ding, L.; Ge, W. K.; Chen, H. Y.; Gwo, S. *Appl. Phys. Lett.* **2006**, *88*, 103107.
(5) Kohan, A. F.; Ceder, G.; Morgan, D.; Van de Walle, C. G. *Phys. Rev. B* **2000**, *61*, 15109.
(6) Borseth, T. M.; Svensson, B. G.; Kuznetsov, A. Y.; Klason, P.; Zhao, Q. X.; Willander, M. *Appl. Phys. Lett.* **2006**, *89*, 262112.
(7) Zhang, D. H.; Xue, Z. Y.; Wang, Q. P. *J. Phys. D: Appl. Phys.* **2002**, *35*, 2837.
(8) Lin, B.; Fu, Z.; Jia, Y. *Appl. Phys. Lett.* **2001**, *79*, 943.
(9) Wei, H.; Wu, Y.; Wu, L.; Hu, C. *Mater. Lett.* **2005**, *59*, 271.
(10) Yang, Y.; Qi, J.; Liao, Q.; Zhang, Y.; Yau, X.; Huang, Y.; Tang, L. *Appl. Phys. A: Mater. Sci. Process.* **2009**, *94*, 799.
(11) Ohashi, N.; Sekiguchi, T.; Aoyama, K.; Ohgaki, T.; Terada, Y.; Sakaguchi, I.; Tsurumi, T.; Haneda, H. *J. Appl. Phys.* **2002**, *91*, 3658.
(12) Van Dijken, A.; Meulenkamp, E. M.; Vanmaekelbergh, D.; Meijerink, A. *J. Lumin.* **2000**, *87*, 454.
(13) Wang, Z. L. *Mater. Sci. Eng., R* **2009**, *64*, 33.
(14) Ahn, M. W.; Park, K. S.; Heo, J. H.; Park, J. G.; Kim, D. W.; Choi, K. J.; Lee, J. H.; Hong, S. H. *Appl. Phys. Lett.* **2008**, *93*, 263103.
(15) Liao, L.; Lu, H. B.; Li, J. C.; Liu, C.; Fu, D. J.; Liu, Y. L. *Appl. Phys. Lett.* **2007**, *91*, 173110.
(16) Baratto, C.; Todros, S.; Faglia, G.; Comini, E.; Sberveglieri, G.; Lettieri, S.; Santamaria, L.; Mabdalena, P. *Sens. Actuators, B* **2009**, *140*, 461.
(17) Van Dijken, A.; Meulenkamp, E. A.; Vanmaekelbergh, D.; Meijerink, A. *J. Phys. Chem. B* **2000**, *104*, 1715.
(18) Van Dijken, A.; Meulenkamp, E. A.; Vanmaekelbergh, D.; Meijerink, A. *J. Phys. Chem. B* **2000**, *104*, 4355.
(19) Wang, Y.; Zhao, F.; Xie, P.; Liang, S.; Deng, S.; Xu, N. *Opt. Commun.* **2007**, *276*, 186.
(20) Djurisic, A. B.; Choi, W. C. H.; Roy, V. A. L.; Leung, Y. H.; Kwong, C. Y.; Cheah, K. W.; Krishnaswamy, T.; Chan, W. K.; Liu, H. F.; Surya, C. *Adv. Funct. Mater.* **2004**, *14*, 856.
(21) Djurisic, A. B.; Leung, Y. H.; Tam, K. H.; Ding, L.; Ge, W. K.; Chen, H. Y.; Gwo, S. *Appl. Phys. Lett.* **2006**, *88*, 103107.
(22) Bahnemann, D. W.; Kormann, C.; Hoffmann, M. R. *J. Phys. Chem.* **1987**, *91*, 3789.
(23) Li, Y.; Meng, G. W.; Zhang, J. D.; Phillipp, F. *Appl. Phys. Lett.* **2000**, *76*, 15.
(24) Wang, L.; Zhang, X.; Zhao, S.; Zhou, G.; Zhou, Y.; Qi, J. *Appl. Phys. Lett.* **2005**, *86*, 024108.
(25) Laudise, R. A.; Ballman, A. A. *J. Phys. Chem.* **1960**, *64*, 688.
(26) Park, W. I.; Kim, D. H.; Jung, S. W.; Yi, G. C. *Appl. Phys. Lett.* **2002**, *80*, 4232.
(27) Li, Y.; Feneberg, M.; Reiser, A.; Schirra, M.; Enchelmaier, R.; Ladenburger, A.; Langlois, A.; Sauer, R.; Thonke, K.; Cai, J.; Rauscher, H. *J. Appl. Phys.* **2006**, *99*, 054307.
(28) Wu, J. J.; Liu, S. C. *J. Phys. Chem. B* **2002**, *106*, 9546.
(29) Wu, C. L.; Chang, L.; Chen, H. G.; Lin, C. W.; Chang, T. F.; Chao, Y. C.; Yan, J. K. *Thin Solid Films* **2006**, *498*, 137.
(30) Liu, X.; Wu, X.; Cao, H.; Chang, R. P. H. *J. Appl. Phys.* **2004**, *95*, 314.
(31) Borras, A.; Cotrino, J.; Gonzalez-Elipe, A. R. *J. Electrochem. Soc.* **2007**, *154*, 12.
(32) Borras, A.; Yanguas-Gil, A.; Barranco, A.; Cotrino, J.; Gonzalez-Elipe, A. R. *Phys. Rev. B* **2007**, *76*, 235303.
(33) Martín, A.; Espinós, J. P.; Justo, A.; Holgado, J. P.; Yubero, F.; González-Elipe, A. R. *Surf. Coat. Technol.* **2002**, *151*, 289–293.
(34) Bekermann, D.; Gasparotto, A.; Barreca, D.; Bovo, L. *Cryst. Growth Des.* **2010**, *10*, 2011.
(35) Zang, Y.; Bahlawane, N. *J. Phys. Chem. C* **2010**, *114*, 5121.
(36) Yang, B.; Kumar, A.; Feng, P.; Katiyar, R. S. *Appl. Phys. Lett.* **2008**, *92*, 233112.
(37) Gracia, F.; Holgado, J. P.; González-Elipe, A. R. *Langmuir* **2004**, *20*, 1688.
(38) Winter, R.; Korzec, D.; Engemann, J. *Surf. Coat. Technol.* **1997**, *91*, 101.
(39) Barranco, A.; Cotrino, J.; Yubero, F.; Espinos, J. P.; Benitez, J.; Clerc, C.; Gonzalez-Elipe, A. R. *Thin Solid Films* **2001**, *410*, 150.
(40) Fang, Z. B.; Yan, Z. J.; Tan, Y. S.; Liu, X. Q.; Wang, Y. Y. *Appl. Surf. Sci.* **2005**, *241*, 303.
(41) Choim, J. H.; Tabatam, H.; Kawaim, T. *J. Cryst. Growth* **2001**, *226*, 493.
(42) Ashrafi, A. B. M. A.; Binh, N. T.; Zhang, B. P.; Segawa, Y. *Appl. Phys. Lett.* **2004**, *84*, 2814.
(43) Voss, T.; Bekeny, C.; Wischmeier, L.; Gafsi, H.; Börner, S.; Schade, W.; Mofor, A. C.; Bakin, A.; Waag, A. *Appl. Phys. Lett.* **2006**, *89*, 82107.
(44) Lima, S. A. M.; Sigoli, F. A.; Jafelicci, M.; Davolos, M. R. *Int. J. Inorg. Mater.* **2001**, *3*, 749.
(45) Shalish, I.; Temkyn, H.; Narayanamurti, V. *Phys. Rev. B* **2004**, *69*, 245401.
(46) Matsumoto, T.; Kato, H.; Miyamoto, K.; Sano, M.; Zhukov, E. A. *Appl. Phys. Lett.* **2002**, *81*, 1231.
(47) Cui, J. *J. Phys. Chem. C* **2008**, *112*, 10385.
(48) Gao, M.; Cheng, R.; Li, W.; Li, Y.; Zhang, X.; Xie, S. *J. Phys. Chem. C* **2010**, *114*, 11081.
(49) Djurisic, A. B.; Leung, Y. H.; Tam, K. H.; Ding, L.; Ge, W. K.; Chen, H. Y.; Gwo, S. *Appl. Phys. Lett.* **2006**, *88*, 103107.
(50) Fan, H. B.; Yang, S. Y.; Zhang, P. F.; Wei, H. Y.; Liu, X. L.; Jiao, C. M.; Zhu, Q. S.; Chen, Y. H.; Wang, Z. G. *Chin. Phys. Lett.* **2007**, *24*, 2108.
(51) Ong, H. C.; Du, G. T. *J. Cryst. Growth* **2004**, *265*, 471.
(52) Malandrino, G.; Blandino, M.; Fragala, M. E.; Losurdo, M.; Bruno, G. *J. Phys. Chem. C* **2008**, *112*, 9595.
(53) Ohashi, N.; Ishigaki, T.; Okada, N.; Taguchi, H.; Sakaguchi, I.; Hishita, S.; Sekiguchi, T.; Haneda, H. *J. Appl. Phys.* **2003**, *93*, 6386.

JP103902U